AGU PUBLICATIONS

JGR

Journal of Geophysical Research: Oceans

RESEARCH ARTICLE

10.1002/2014JC010547

Key Points:
- The SST in the first half of 2012 was the highest ever recorded
- Atmospheric circulation in the preceding winter caused the extreme warm anomaly
- Ocean advection is secondary during this extreme event

Correspondence to:
K. Chen,
kchen@whoi.edu

Citation:
Chen, K., G. Gawarkiewicz, Y.-O. Kwon, and W. G. Zhang (2015), The role of atmospheric forcing versus ocean advection during the extreme warming of the Northeast U.S. continental shelf in 2012, *J. Geophys. Res. Oceans*, *120*, 4324–4339, doi:10.1002/2014JC010547.

Received 27 OCT 2014
Accepted 25 MAY 2015
Accepted article online 29 MAY 2015
Published online 15 JUN 2015

The role of atmospheric forcing versus ocean advection during the extreme warming of the Northeast U.S. continental shelf in 2012

Ke Chen[1], Glen Gawarkiewicz[1], Young-Oh Kwon[1], and Weifeng G. Zhang[2]

[1]Physical Oceanography Department, Woods Hole Oceanographic Institution, Woods Hole, Massachusetts, USA, [2]Applied Ocean Physics and Engineering Department, Woods Hole Oceanographic Institution, Woods Hole, Massachusetts, USA

Abstract In the coastal ocean off the Northeast U.S., the sea surface temperature (SST) in the first half of 2012 was the highest on the record for the past roughly 150 years of recorded observations. The underlying dynamical processes responsible for this extreme event are examined using a numerical model, and the relative contributions of air-sea heat flux versus lateral ocean advective heat flux are quantified. The model accurately reproduces the observed vertical structure and the spatiotemporal characteristics of the thermohaline condition of the Gulf of Maine and the Middle Atlantic Bight waters during the anomalous warming period. Analysis of the model results show that the warming event was primarily driven by the anomalous air-sea heat flux, while the smaller contribution by the ocean advection worked against this flux by acting to cool the shelf. The anomalous air-sea heat flux exhibited a shelf-wide coherence, consistent with the shelf-wide warming pattern, while the ocean advective heat flux was dominated by localized, relatively smaller-scale processes. The anomalous cooling due to advection primarily resulted from the along-shelf heat flux divergence in the Gulf of Maine, while in the Middle Atlantic Bight the advective contribution from the along-shelf and cross-shelf heat flux divergences was comparable. The modeling results confirm the conclusion of the recent analysis of in situ data by Chen et al. (2014a) that the changes in the large-scale atmospheric circulation in the winter of 2011–2012 primarily caused the extreme warm anomaly in the spring of 2012. The effect of along-shelf or cross-shelf ocean advection on the warm anomalies from either the Scotian Shelf or adjacent continental slope was secondary.

1. Introduction

Recent studies suggest that the severity and frequency of extreme events in global and regional systems have been increasing, and these changes are potentially related to anthropogenic climate change [*Coumou and Rahmstorf*, 2012; *Hansen et al*., 2012; *Rahmstorf and Coumou*, 2011]. Record drought, extreme warm anomalies, extreme low sea-ice extent, anomalous rainfall, and a super hurricane have been reported around the globe in 2011–2012 [*Peterson et al*., 2013]. In the coastal ocean off the Northeast U.S., the sea surface temperature (SST) in the first half of 2012 was the highest on record (Figure 1) [*Friedland*, 2012]. The magnitude of the anomaly was 3–4°C and exceeded 3 standard deviations (Figure 2) in the Gulf of Maine (GoM) and the Middle Atlantic Bight (MAB). In addition, *Gawarkiewicz et al*. [2012] reported near-bottom temperature anomalies exceeding 4°C in November–December 2011 in the outer shelf near the southern flank of Georges Bank. The temperature change resulted in significant impacts on the marine ecosystem [*Mills et al*., 2013], such as an observed northward shift in the distribution of Atlantic cod in this region [*Friedland*, 2012]. Commercial fishermen also reported an increased abundance of squid in the summer of 2012, as well as the appearance of warm water species not previously seen off southern New England such as cobia and grouper [*Gawarkiewicz et al*., 2013]. Understanding the cause of such an extreme event on the coastal ocean and unraveling the underlying dynamics are important for better fisheries management and adaptation during a time of rapid change, as well as for exploring the seasonal predictability of the thermal structure in the coastal ocean.

Chen et al. [2014a] recently identified a significant covariability between the winter atmospheric jet stream latitude and ocean temperature anomalies on the continental shelf in the MAB over the last 30 years. For example, the jet stream latitudinal position along 70°W was at an extreme northern position in 2012. Using

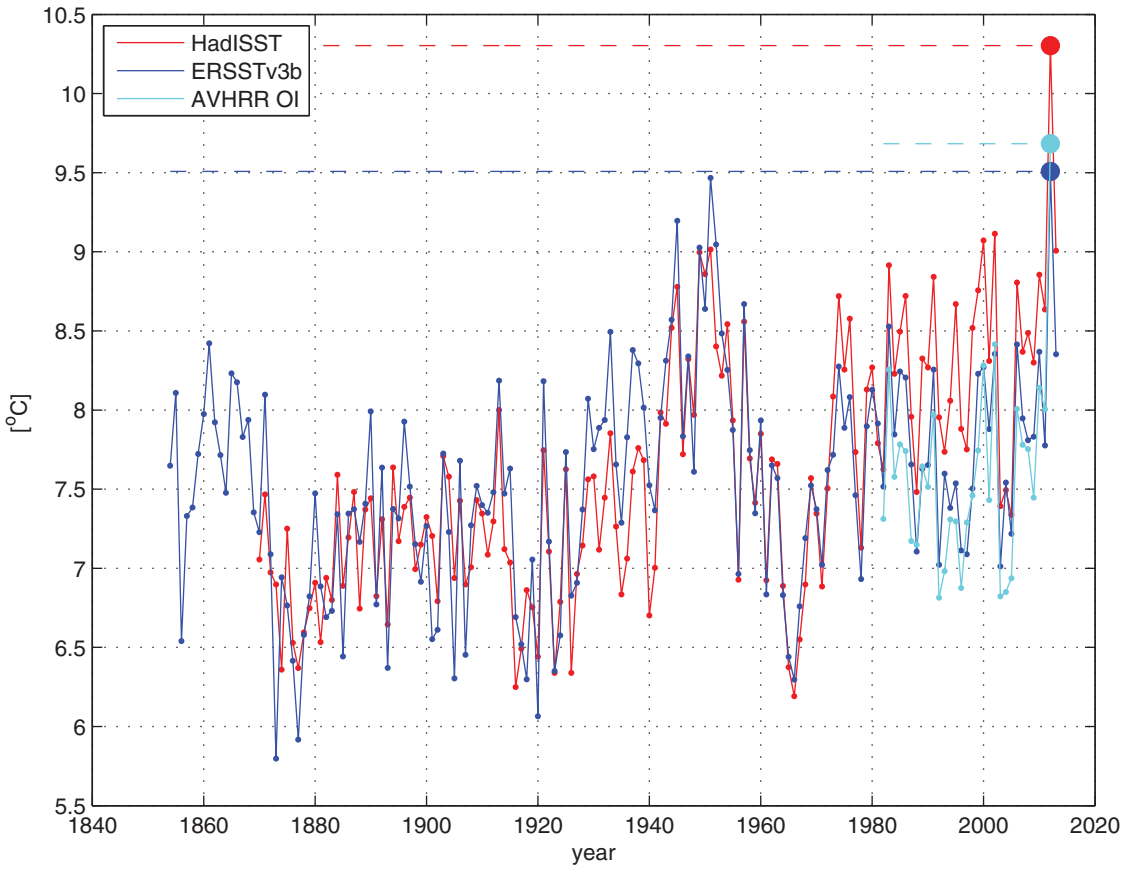

Figure 1. Spatial mean SST in the Middle Atlantic Bight and Gulf of Maine averaged over January–June. The spatial mean SST was calculated by averaging original data within the MAB and GoM regions defined in Figure 2, which covers the entire continental shelf from Nova Scotia to Cape Hatteras. The spatial mean SST in the first half of 2012 is shown by closed circles for each data set. The Hadley Center Sea Ice and SST data set version 1 (HadISST), NOAA Extended Reconstructed SST version 3b (ERSSTv3b), and NOAA Optimum Interpolation SST (AVHRR OI) are shown in red, blue, and cyan, respectively. See section 2.2 for the details of the data sets.

available observations, they found that the anomalous air-sea heat flux associated with the northward shift of the jet stream reduced the cooling rate of the ocean during the winter of 2011–2012, and that the SST anomalies in the spring of 2012 exhibited an intraseasonal oscillation strongly correlated with the jet stream latitude variability. This work indicates that air-sea heat exchange plays an important role in regulating heat content on the shelf. However, previous studies have demonstrated that long-term changes in ocean temperature in the region are best explained by along-shelf ocean advection [e.g., *Lentz*, 2010; *Shearman and Lentz*, 2010]. In addition, shelf-slope exchange processes at the edge of the continental shelf [e.g., *Chen et al.*, 2014b; *Garvine et al.*, 1989; *Gawarkiewicz et al.*, 2004], particularly under the strong influence of the Gulf Stream [*Gawarkiewicz et al.*, 2012], are another potentially important player in determining the shelf temperature budget. The limited availability of in situ observations has hampered a complete quantification of the heat budget on the northeast U.S. continental shelf. In particular, the relative size of air-sea heat flux, along-shelf advective heat flux, and cross-shelf edge heat exchange remains unclear due to the complexity of processes contributing to temperature changes in the coastal ocean. This also hindered the understanding of the relative contributions from the atmosphere and the ocean on the coastal warming event in the winter of 2011–2012.

In this study, we conduct numerical modeling to unravel the dynamics underlying the extreme warming in the Northeast U.S. coastal ocean. Specifically, we quantify the heat balances in the GoM and the MAB and quantify the relative contributions between the air-sea flux and the ocean advective heat flux during the extreme warm anomaly in 2012. Better understanding of this unprecedented event will provide insights into the interannual variability of temperature in the Northeast U.S. coastal ocean.

We provide, in section 2, a description of the model configuration, the forcing, and the data used for the verification of the model thermal structure. The performance of the model is evaluated in section 3 with

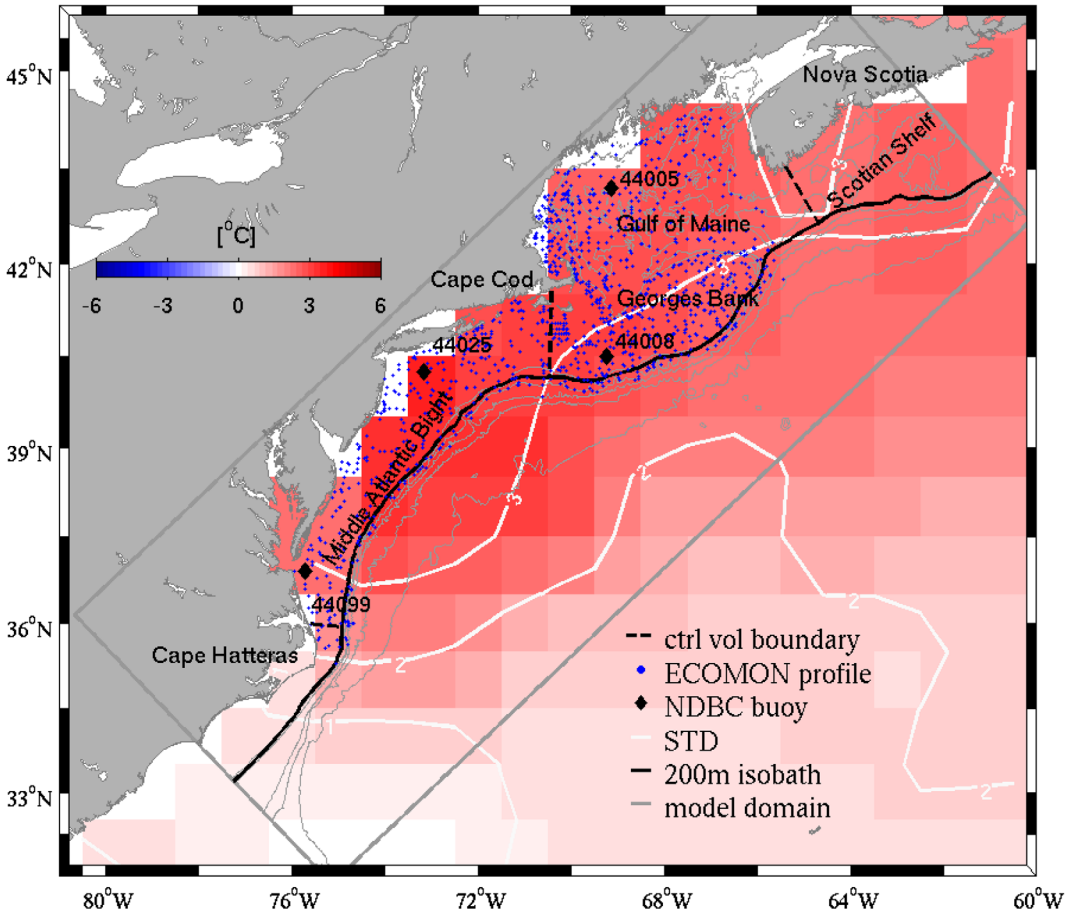

Figure 2. Map showing the SST anomaly (in color) in January–June 2012 in the Northeast coastal ocean and the model domain (gray rectangle). SST anomaly is based on HadISST with a reference being January–June average SST during 1870–2013, and white contours represent standard deviations. Locations of NDBC buoys are shown by black diamonds. Locations of temperature and salinity profiles from the NEFSC ECOMON program are shown in blue dots. The smoothed 200 m isobath (black curve) and black dashed lines represent the boundary of the control volumes for the Gulf of Maine (GoM) and the Middle Atlantic Bight (MAB). These two regions are used for the calculation of spatial mean SST shown in Figure 1. The gray contours are 100, 200, 1000, 2000, and 3000 m isobaths.

statistical measures of the mismatch between the model results and observations. Section 4 discusses the heat balance of the Northeast coastal ocean during 2011–2012. Section 5 focuses on the diagnostics of the temperature anomaly and reveals the interplay of the atmospheric and oceanic processes. A summary is provided in section 6.

2. Model Configuration and Data for Comparison

2.1. Model Setup and Numerical Treatment

The modeling philosophy is to design a realistic regional model that is able to capture the circulation dynamics on the shelf with imposed mesoscale circulation in the open ocean. The imposed realistic mesoscale variability in the open ocean is based on a combination of a data-assimilative global ocean model output and a temporal mean field from an observational climatology. The open boundary conditions of a realistic regional ocean model are intrinsically ill-posed (due to incomplete knowledge of the ocean outside the model domain), and the length scales of nonlinear mesoscale dynamics in the open ocean (O(100 km)) are not much smaller than the spatial coverage of our regional model (Figure 2). Therefore, resolving the exact mesoscale circulation in the open ocean for a particular time period is difficult for the regional model. Our approach (introduced below in this section) of imposing mesoscale variability in the open ocean from a data-assimilative global model circumvents this difficulty and allows the realistic mesoscale circulation in

the open ocean to influence the simulated shelf processes. This meets the objective of this study to quantify the temperature budget on the shelf.

The model utilized in this study is a shelf-wide ocean circulation model, based on the hydrostatic Regional Ocean Modeling System (ROMS). The ROMS is a free-surface, primitive equation model in widespread use for estuarine, coastal, and basin-scale ocean applications (www.myroms.org/papers). ROMS employs split-explicit separation of fast barotropic and slow baroclinic modes and is formulated in vertically stretched terrain-following coordinates using algorithms described in detail by *Shchepetkin and McWilliams* [2005] and *Haidvogel et al*. [2008]. A redefinition of the barotropic pressure-gradient term [*Shchepetkin and McWilliams*, 2005] is also applied in ROMS to reduce the pressure-gradient truncation error. Our regional model domain encompasses both the MAB and GoM (hereinafter, MABGOM model), bounded by Cape Hatteras in the southwest and Nova Scotia in the northeast (Figure 2). The model's horizontal resolution is 10 km in the along-shelf direction, and 6 km in the cross-shelf direction. Vertically, there are 36 terrain-following levels in the water column with higher resolution near the surface and bottom in order to better resolve ocean boundary layers. A generic-length scale (GLS) turbulent mixing closure k-kl scheme [*Warner et al*., 2005] was used to calculate vertical mixing, and bottom stress was computed using a quadratic method with a drag coefficient of 0.003.

For the surface forcing of the model, we employ a scheme that combines air-sea flux calculated using bulk formulae and a surface thermal correction based on high-resolution SST maps. This scheme has been applied previously to provide realistic forcing of air-sea exchange [*Chen and He*, 2010]. The bulk formulae calculation [*Fairall et al*., 2003] is based on three hourly and 35 km resolution meteorological data (surface winds, air temperature, air pressure, relative humidity, short wave radiation, long wave radiation, cloud coverage, and precipitation) from the National Center for Environment Prediction (NCEP) North America Regional Reanalysis (NARR). This calculation provides large-scale variability in the fluxes of momentum and buoyancy at the ocean surface but is incapable of reproducing some fine scale structures due to low spatial resolution of the meteorological data. To compensate for this deficiency in the surface forcing, the surface thermal correction adjusts the surface heat flux based on the difference of the model SST and the 1 km resolution Multi-scale Ultra-high Resolution (MUR) SST. The adjustment time scale is 3 h, consistent with the temporal resolution of the NARR product. Additional sensitivity experiments with shorter and longer (including indefinite) adjustment time scales indicate that the major results discussed in sections 4 and 5 are not sensitive to the adjustment time scale.

Fresh water runoff from nine major rivers in the region was also imposed. These include the St. John, Penobscot, Kennebec, Androscoggin, Merrimack, Connecticut, Hudson, Delaware, and Potomac Rivers. For each river, United State Geological Survey (USGS) real-time runoff measurements were used to specify freshwater volume transport and temperature.

The model initial conditions are extracted from a product that combines the mesoscale variability from a data-assimilative global ocean circulation model, Hybrid Coordinate Ocean Model [*Chassignet et al*., 2006] plus Navy Coupled Ocean Data Assimilation (HYCOM/NCODA), with the background mean fields from the temperature and salinity climatology of the World Ocean Atlas (WOA) 2013. The HYCOM/NCODA data set (publicly available at: https://hycom.org) provides daily prognostic ocean state variables on a 1/12° horizontal grid with 33 depth levels. Due to the limitation of grid resolution and missing dynamics (e.g., river inflow) of global models in the coastal region, the HYCOM/NCODA data set has a systematic temperature and salinity bias, particularly on the continental shelf. We corrected the HYCOM/NCODA data against the temperature and salinity climatology from the World Ocean Atlas (WOA) 2013. Removing the mean bias is especially important in this study in which we aim to diagnose the temperature budget on the shelf. WOA 2013 provides a climatology for 1955–2012 and also a climatology for 2005–2012. We found that correction of temperature and salinity based on the 2005–2012 climatology gave more realistic results, as the HYCOM/NCODA data set we used is for 2004–2014. This correction is particularly important considering the long-term warming trend in the Northeast coastal ocean (Figure 1). In the correction, the climatological monthly means of temperature and salinity from the HYCOM/NCODA data set were replaced by climatological monthly means from the WOA while the variability, i.e., the deviations from the climatological mean, was retained. Similarly, the mean dynamic height and associated geostrophic transport were computed along the southwestern and northeastern boundaries based on the WOA monthly mean temperature and salinity. Then, the monthly mean dynamic height and geostrophic transport from HYCOM/NCODA were corrected

by their counterparts from the WOA climatology. In doing so, we remove the mean biases in the hydrography used for the boundary condition in a dynamically consistent way.

Temperature and salinity from the open ocean (deeper than 2000 m) in the MABGOM model were nudged back to the corrected, four dimensional temperature/salinity field from HYCOM/NCODA. The nudging time scale is 2 days at the open boundary and increases linearly to a very long time scale (1000 days) at the 2000 m isobath, which results in nudging strength decreasing gradually from the open boundary toward the interior. No nudging was applied in regions of water depth shallower than 2000 m. Generally, the data-assimilative HYCOM/NCODA provides good estimates of the mesoscale variability in the open ocean, particularly on the formation of Gulf Stream meanders and the location and intensity of warm core rings in the Slope Sea. With the temperature and salinity nudging in the Gulf Stream/Slope Sea region, the model is able to realistically capture the meandering of the Gulf Stream and the hydrography in the Slope region and is able to provide vital information for estimating the cross-shelf heat flux. The 2000 m isobath generally follows the orientation of the shelf break ($\sim$200 m isobath), and the distance between the shelf break and 2000 m isobath varies from 50 to70 km, larger than the characteristic spatial scales (10–30 km) in this region [*Todd et al*., 2012]. Therefore, the nudging only constrains conditions in the open ocean and allows dynamical processes to evolve freely exchanging water masses between the open ocean and the shelf.

Subtidal free-surface and 2-D momentum boundary conditions of the MABGOM model were derived from the corrected HYCOM/NCODA fields using an explicit Chapman [*Chapman*, 1985] and Shchepetkin scheme [*Mason et al*., 2010], plus M2 tidal harmonics from an Advanced Circulation Model for Oceanic, Coastal and Estuarine Waters (ADCIRC) tidal simulation of the western Atlantic [*Luettich et al*., 1992]. An Orlanski-type radiation [*Orlanski*, 1976] boundary condition was used for 3-D state variables.

Focusing on the extreme warming event during winter 2011–2012, we performed a hindcast simulation from September 2011 to December 2012, covering the anomalous conditions during winter-spring [*Chen et al*., 2014a]. To quantify the mean conditions, we also ran the MABGOM model for 10 years continuously from 2004 to 2013, using the same configuration as the 2012 run, to produce long-term means of fluxes that are representative of normal conditions.

2.2. Data

Three gridded SST data sets were used to characterize the warm anomaly in 2012 (Figures 1 and 2). The first data set is the Hadley Center Sea Ice and SST (HadISST) version 1 from UK Met Office Hadley Centre for Climate Prediction and Research. HadISST is a combination of data from the Met Office Marine Data Bank (mostly ship tracks), Global Telecommunications System (GTS), International Comprehensive Ocean-Atmosphere Data Set (ICOADS), and Advanced Very High Resolution Radiometer (AVHRR) satellite SST using optimal interpolation [*Rayner et al*., 2003]. The data are available monthly from 1870 to the present with a spatial resolution of $1^\circ \times 1^\circ$ (http://www.metoffice.gov.uk/hadobs/hadisst/). The second data set is the Extended Reconstructed Sea Surface Temperature version 3b data (ERSSTv3b) from the National Oceanic and Atmospheric Administration (NOAA) Earth System Research Laboratory. The data are combinations of ICOADS ship and buoy data and NCEP GTS SST [*Smith et al*., 2008] and are available monthly from 1854 to the present on a $2^\circ \times 2^\circ$ grid (http://www.esrl.noaa.gov/psd/data/gridded/data.noaa.ersst.html). The third data set is the NOAA Optimum Interpolation SST, based on AVHRR satellite measurements [*Reynolds et al*., 2007] and is available daily from 1981 to the present at 1/4° resolution (http://www.ncdc.noaa.gov/sst/).

We also use the Multi-scale Ultra-high Resolution (MUR) SST from Jet Propulsion Laboratory (JPL) for surface thermal correction (see section 2.1). MUR SST is part of the Group for High Resolution Sea Surface Temperature (GHRSST) and provides 1 km gridded data from 2002 to present on a daily basis. Near-surface temperature data from 4 National Data Buoy Center (NDBC) buoys within the MAB and GoM (see Figure 2 for the locations) are used to compare against the model simulation. These buoys are located in the GoM (44005), on the continental shelf near Nantucket (44008), Long Island (44025), and Virginia Beach (44099). Temperature and salinity profiles from the Ecosystem Monitoring (ECOMON) program of the NOAA Northeast Fisheries Science Center (NEFSC) are also used. ECOMON surveys are conducted 6–7 times per year, providing valuable hydrographic data with fairly complete coverage of the continental shelf in the region (Figure 2).

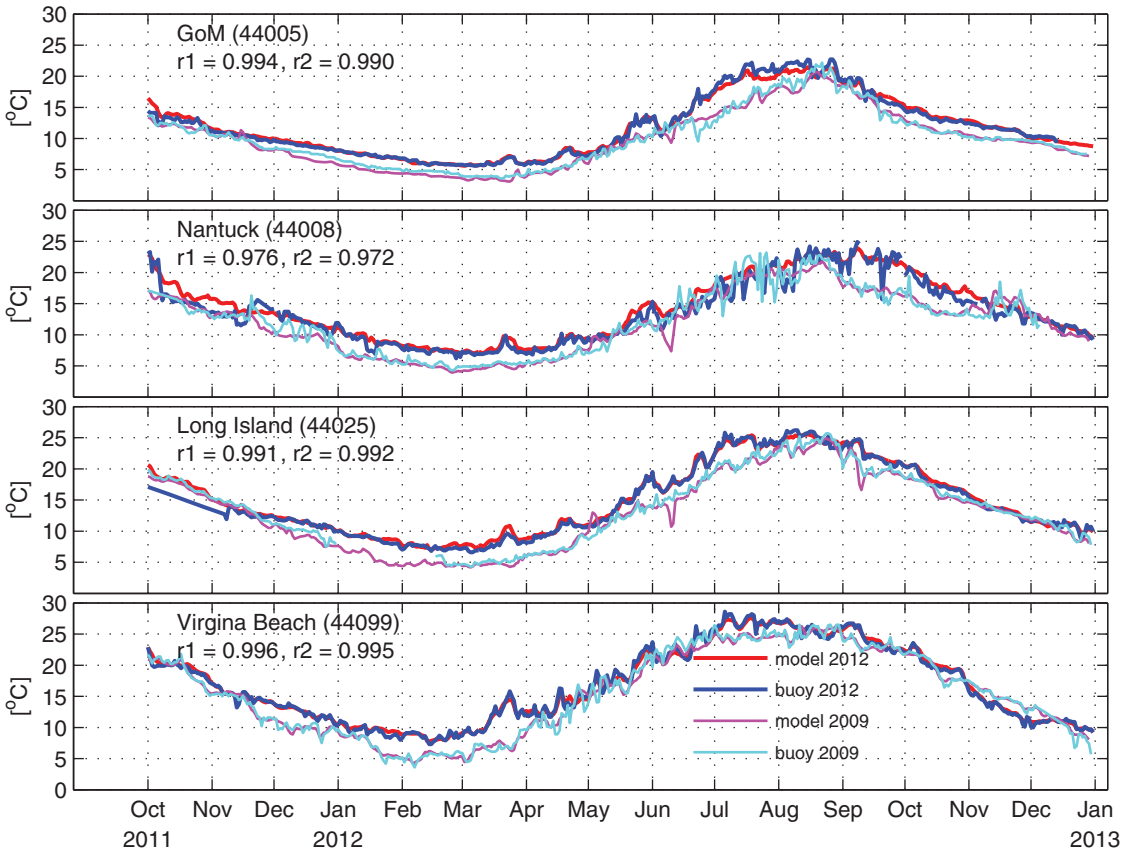

Figure 3. Comparison of surface temperature between NDBC buoys (blue and cyan) and the model (red and magenta) at four NDBC buoys during 2008–2009 and 2011–2012. Time series during 2011–2012 (red and blue) and 2008–2009 (magenta and cyan) are both plotted for comparison. Linear correlation coefficients between the modeled and observed time series (r1 for 2011–2012 and r2 for 2008–2009) are shown.

3. Model-Data Comparison

Extensive model/observation comparisons in a previous study using the similar model configuration indicate that the MABGOM model is able to successfully reproduce the temporal and spatial variability of the regional circulation during 2004–2013 [*Chen and He*, 2014]. In the previous studies, the MABGOM model successfully provided open boundary conditions for a higher-resolution model [*Chen and He*, 2010] that focused on MAB shelfbreak processes.

For this study, we further validated the model against available observations during 2011–2012. To realistically simulate the shelf thermal structure and its evolution, we first compare the model solution against temperature measured at four NDBC buoys. The water temperature recorded at the buoy represents the temperature in the upper water column as opposed to skin temperature. This is comparable to the temperature in the top layer of the model. As shown in Figure 3, our model hindcast accurately reproduced both the seasonal cycle and much of the short-term fluctuations of surface temperature during 2011–2012. Linear correlation coefficients range from 0.976 to 0.996, above the 99% confidence level. In particular, the model clearly captures the intraseasonal oscillations of surface temperature in March–May 2012. For comparison, we also show the surface temperature records during the same period of 2008–2009, during which the thermal condition in the GoM and the MAB is close to the long-term mean. Again, the model successfully captures the surface thermal conditions with correlations above 0.97, significant at the 99% confidence level. Of interest is the large interannual change of surface temperature between the two periods: during the winter of 2011–2012, the surface water did not cool as much as in 2008–2009, and the maximum temperature difference is ~5°C. The preceding thermal conditions in winter 2011–2012 favored the warming in the following season. The anomalously positive air-sea heat flux in spring 2012 further induced the record warm condition in the first half of 2012 [*Chen et al.*, 2014a].

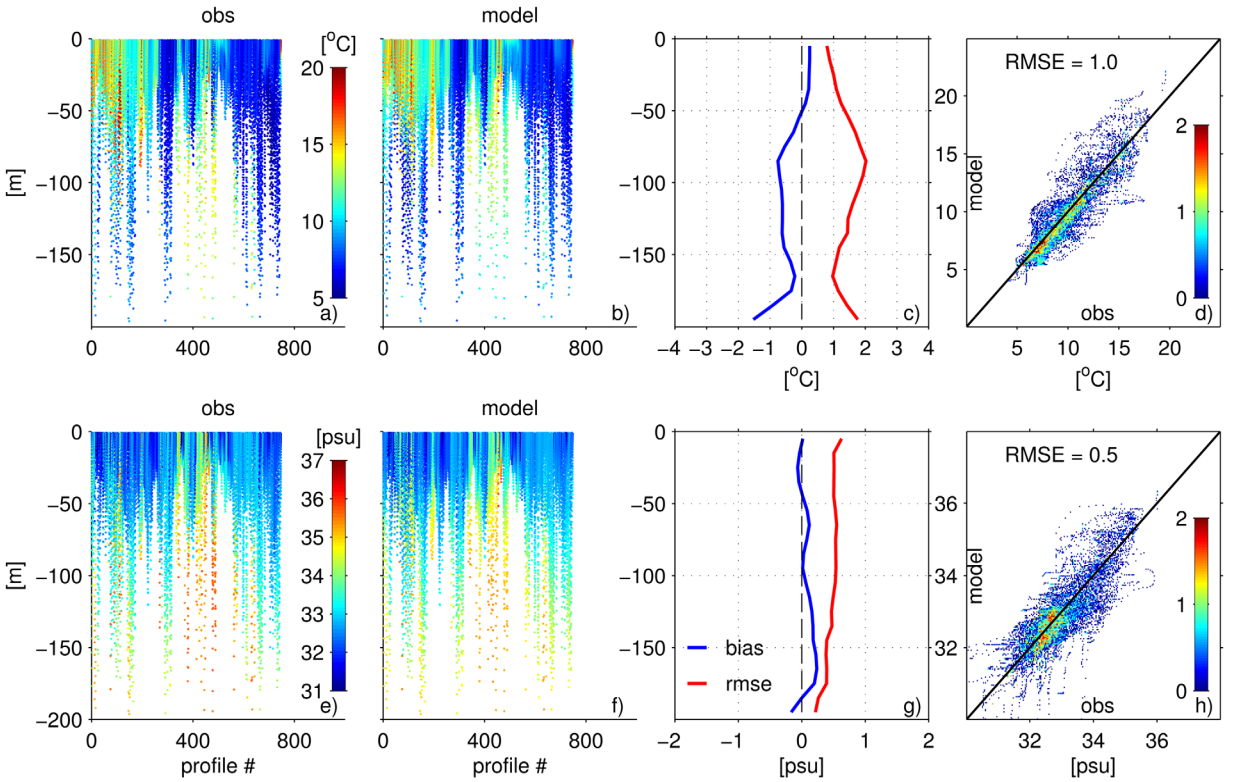

Figure 4. Comparisons of observed (a) temperature and (e) salinity profiles and (b, f) the model counterparts (respectively). Profiles are sorted in time-ascending order from 1 November 2011 to 31 May 2012. (c, g) Vertical distribution of mean bias (model minus observation) and RMS error. (d, h) One-on-one plots showing the overall comparison between the observation and the model. Colorbars in Figures 4d and 4h are in the logarithmic scale for the number of points in each 0.1°C × 0.1°C box and 0.03 psu × 0.03 psu box, respectively.

A more rigorous way to validate the performance of the model is to compare the subsurface hydrographic profiles (Figure 4). The temperature and salinity profiles were sorted in a time-ascending order. The first profile was taken on 1 November 2011, and the last profile was on 31 May 2012. Note that the spatial locations of the profiles vary, so the profiles shown in Figure 4 do not represent seasonal evolution at a specific location. The thermal structure on the Northeast continental shelf has strong spatiotemporal variations, and the model captured this characteristic very well. Over the water column, the model underestimated the temperature by less than 1°C, mostly at depths below 50 m, and the temperature bias decreases toward the surface. Root-mean-square error (RMSE) of the model ranges from less than 1°C at the ocean surface to ~2°C around 80 m and deeper. The overall RMSE is 1°C between the observation and model, which is consistent with the performance of state of the art non-data-assimilative models [*Wilkin and Hunter*, 2013]. Similarly, the model also captures the observed spatiotemporal variation of salinity over the water column during winter-spring of 2011–2012. Salinity bias of the model is close to 0 in the upper 100 m and is less than 0.3 in deep water. Salinity RMSE decreases from ~0.5 at the surface to ~0.2 at 200 m. For all realizations, the salinity RMSE of the model between the model and observations is 0.5, which again represents a similar model skill as other numerical models for this region.

4. Depth-Averaged Temperature Budget

An earlier study suggested that the shelf-wide warm anomaly started in November 2011 and continued into the first half of 2012 [*Chen et al*., 2014a]. In particular, the positive (i.e., from atmosphere to ocean) heat flux anomaly induced by the northward shift of the jet stream reduced the seasonal cooling rate of ocean temperature in the winter of 2011–2012. This anomaly in air-sea fluxes during winter preconditioned the extreme ocean warming in the spring of 2012. Based upon these findings, it is important to investigate the temperature budget during the winter (cooling) and spring (warming) periods.

The calculation of oceanic heat transport (unit: W) across a nonclosed section requires a reference temperature (temperature scale, Kelvin or Celsius) [*Hall and Bryden*, 1982; *Montgomery*, 1972], and comparison of heat transport between two different stand-alone sections is less meaningful [*Schauer and Beszczynska-Möller*, 2009]. In the following, our calculations focus on the temperature budget diagnostics on the control volumes of the GoM and MAB, thus the ocean advective heat flux (W m^{-2}) across lateral boundaries can be directly compared. For the convenience of discussion, we transform and refer the advective heat flux to depth-averaged temperature advection (°C s^{-1}, section 4), as well as volume-averaged temperature advection (°C s^{-1}, section 5) and temperature transport (°C m^3 s^{-1}, equation (5)). Since these terms are diagnosed for the budget closure of the control volume, they can be discussed equivalently without ambiguity.

Neglecting horizontal diffusion, the depth-averaged temperature balance can be written as

$$\frac{1}{H}\int_{-h}^{\eta}\left(\frac{\partial T}{\partial t}\right)dz+\frac{1}{H}\left(\int_{-h}^{\eta}(\mathbf{u}\cdot\nabla T)dz+\int_{-h}^{\eta}w\frac{\partial T}{\partial z}dz\right)=\frac{Q}{\rho C_p H} \tag{1}$$

where T is four-dimensional temperature, $\mathbf{u}$ is the horizontal velocity vector, w is the vertical velocity, $H=h+\eta$ is the total local water depth (while h is bottom depth and η is surface elevation), Q is the net air-sea heat flux, ρ is water density, and C_p is the specific heat capacity. Equation (1) can be expressed as

$$\bar{T}_{rate}=Q_{air}+Q_{hadv}+Q_{vadv} \tag{2}$$

and then temporal integration of (2) gives

$$d\bar{T} = Q_{airT} + Q_{hadvT} + Q_{vadvT} \tag{3}$$

where $\bar{T}$ is the depth-averaged temperature, $Q_{airT}=\int_0^t Q_{air}dt'=\int_0^t\frac{Q}{\rho C_p H}dt'$, $Q_{hadvT}=\int_0^t Q_{hadv}dt'=-\frac{1}{H}\int_0^t\int_{-h}^{\eta}(\mathbf{u}\cdot\nabla T)dzdt'$, and $Q_{vadvT}=\int_0^t Q_{vadv}dt'=-\frac{1}{H}\int_0^t\int_{-h}^{\eta}w\frac{\partial T}{\partial z}dzdt'$

The budget is examined in terms of both instantaneous time rate of change (equation (2)) averaged separately over the cooling and warming period (Figure 5) and the cumulative change (equation (3)) since 1 November 2011 (Figure 6). Note also that the temperature budget is based on the total values including the mean seasonal cycle. Contribution from the neglected term in the temperature budget is small as can be seen from the dashed curve in Figure 6.

During November 2011 to February 2012, the entire water column on the Northeast continental shelf was cooling, primarily reflecting the mean seasonal cycle (Figure 5). The cooling rate ($\bar{T}_{rate}$) ranges from ~0.01°C/d in the central GoM to ~0.07°C/d on Georges Bank and the shallower middle to inner shelf in the MAB. The spatial pattern of the net air-sea heat flux (Q_{air}) largely resembles the time rate of change of depth-averaged temperature. This indicates that the water temperature is primarily a one-dimensional balance, consistent with the findings of previous studies in the region [*Brink et al*., 2009; *Lentz et al*., 2003]. Compared to $\bar{T}_{rate}$ and Q_{air}, the horizontal advective flux (Q_{hadv}) during the cooling period shows more spatial variability. Ocean advection was warming most parts of the inner shelf as a result of the positive temperature gradient from the inner shelf to the outer shelf during this time of the year. In contrast, the horizontal advection was cooling the water column over the outer shelf, the southern flank of Georges Bank and the central GoM.

In the following warming period (March–May 2012), the warming rate of the water column varies from 0.01°C/d in the eastern GoM and outer shelf in the MAB to 0.06°C/d on the inner shelf and Georges Bank. Similarly, this spatial pattern is largely controlled by Q_{air}. During this period, the ocean advective heat flux was cooling most of the region with magnitudes of 0.01–0.2°C/d.

Considering the spatial differences in each term, we further investigate the cumulative heat balance in five subregions (Figure 6). The subregions are selected based on the NEFSC survey polygons, including GoM East, GoM West, Georges Bank, MAB North, and MAB South (Figure 5d). In all subregions, the temperature change over the seasonal time scale is largely controlled by the net air-sea heat flux, especially in the western GoM. From November 2011 to March 2012, the air-sea heat flux was cooling the water column. Ocean advective flux, being smaller in magnitude, also contributed to the cooling. Therefore, $d\bar{T}$ is larger than Q_{airT}

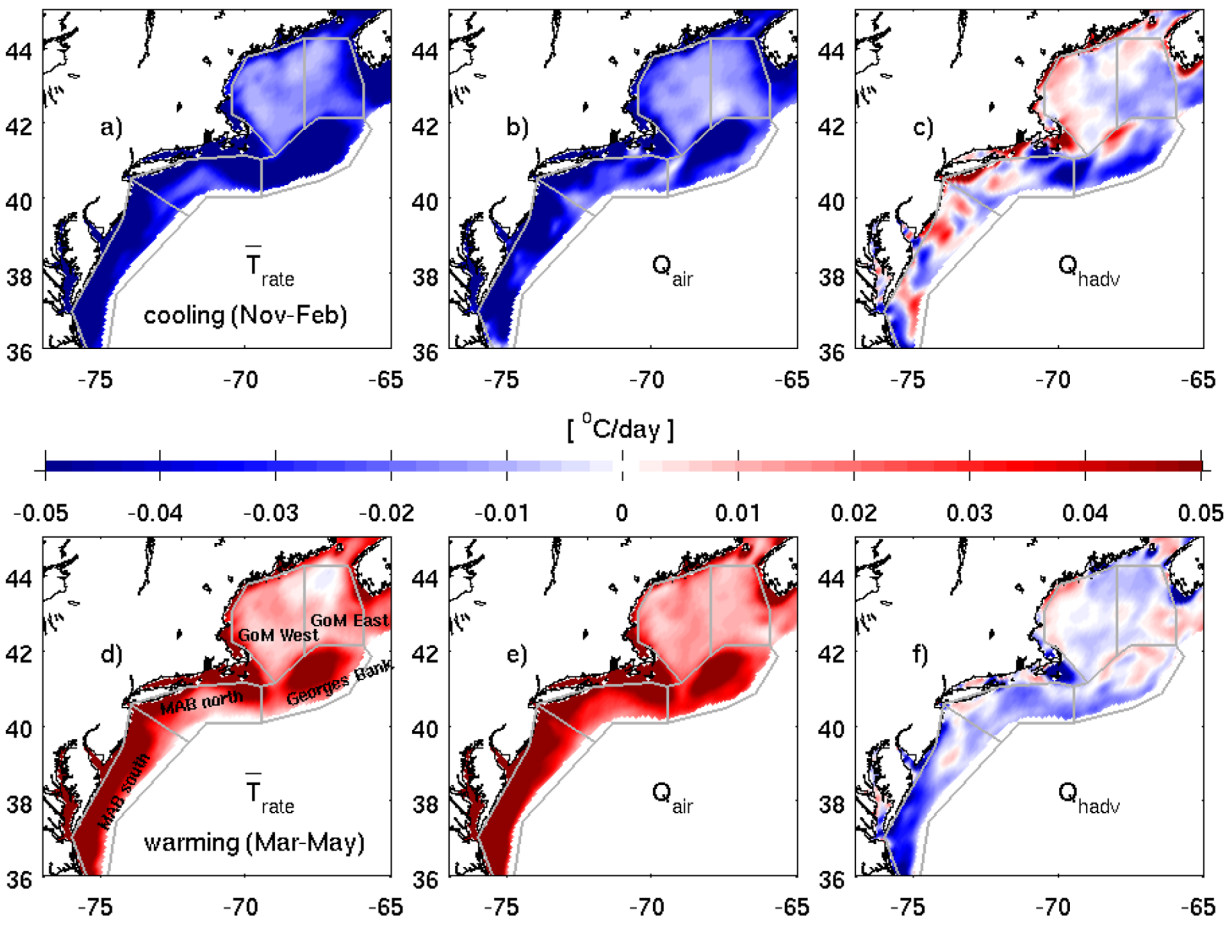

Figure 5. Depth-averaged temperature budget terms on the continental shelf (shoreward of the 200 m isobath) in terms of instantaneous rate of change averaged for cooling and warming periods during 2011–2012, respectively, based on equation (2) in the text: (a, d) time rate of change ($\overline{T}_{rate}$), (b, e) net air-sea heat flux (Q_{air}), and (c, f) horizontal ocean advective flux (Q_{adv}). In each figure, NEFSC survey polygons are shown in gray, with the respective subregions defined in Figure 5d.

during this period. However, during the subsequent warming season, ocean advection was cooling the water column in all subregions, counteracting the air-sea heat flux. This confirms the dominant role the atmospheric forcing played during the extreme warming event of 2011–2012 [*Chen et al*., 2014a].

5. Temperature Anomaly Diagnostics

The analysis in section 4 focused on the total temperature budget during 2011–2012, and the information of the mean seasonal cycle was retained. Therefore, the signals of the mean seasonal cycle dominated the changes in temperature. To better understand what roles the atmosphere and ocean played in producing such an extreme warm anomaly, we need to focus on the temperature anomaly diagnostics, i.e., the deviations from the climatological mean seasonal cycle. Therefore, knowledge of the normal (long-term mean) conditions of both air-sea heat flux and ocean advective heat flux is necessary. We use the mean condition from the 10 year hindcast as the reference to compare with the warm anomaly in 2011–2012. We will focus on the GoM and the MAB separately (see the black dashed lines for the geographic boundaries in Figure 2). For a control volume, the volume-averaged temperature budget can be approximated as

$$\tilde{T}_{rate} = \tilde{Q}_{adv} + \tilde{Q}_{air} \tag{4}$$

where $\tilde{T}_{rate}$ is the time rate of change term for volume-averaged temperature and $\tilde{Q}_{air} = \frac{1}{V_0} \int_{y_1}^{y_2} \int_{x_1}^{x_2} (Q_{air} H) dxdy$ and $\tilde{Q}_{adv} = \frac{1}{V_0} \int_{y_1}^{y_2} \int_{x_1}^{x_2} (Q_{adv} H) dxdy$ are the volume-averaged (over V_0) terms for air-sea heat flux and ocean advective heat flux, respectively.

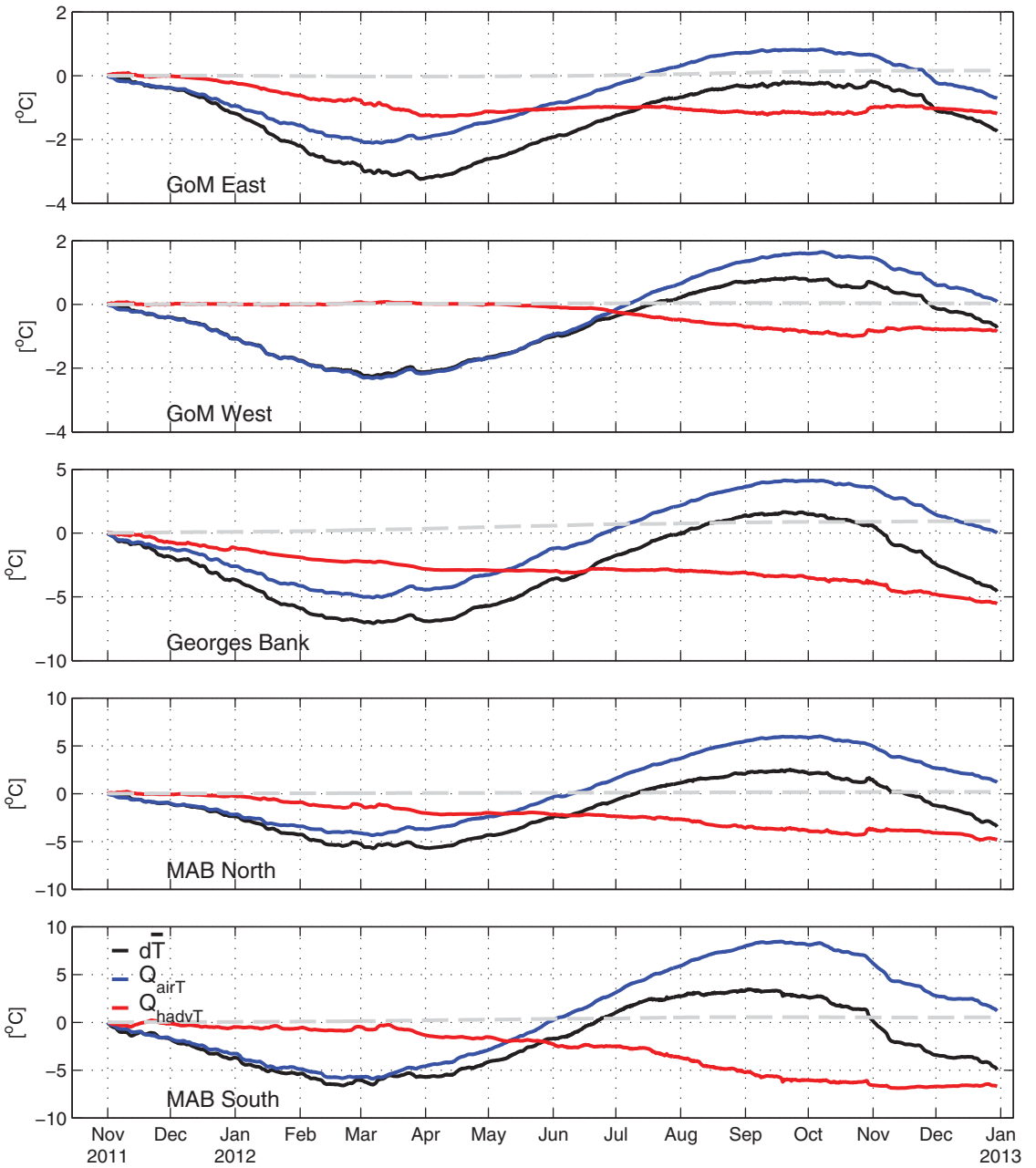

Figure 6. Cumulative depth-averaged temperature budget terms based on equation (3) in the text since 1 November 2011 averaged in the five subregions defined by the NEFSC polygons (Figure 5d). The temperature change, cumulative air-sea flux, and horizontal advective flux are shown in black, blue, and red, respectively. The dashed gray line represents the residuals.

In the GoM, the 10 year mean time rate of change of the volume-averaged temperature ($\tilde{T}_{rate}$) varies from 0.04°C/d in June–July to −0.05°C/d in January–February (Figure 7). Compared to the mean conditions, the $\tilde{T}_{rate}$ during November 2011 to March 2012 was anomalously weak during the cooling period. The positive anomaly of $\tilde{T}_{rate}$ ranges from 0 to 0.02°C/d during this period, indicating the GoM water was cooling more slowly than normal. Similarly, the net air-sea heat flux was also anomalously positive during the cooling period of 2011–2012. Furthermore, both the magnitude and phase of the $\tilde{Q}_{air}$ anomaly are similar to those of the $\tilde{T}_{rate}$, and the linear correlation between the anomalies of $\tilde{T}_{rate}$ and $\tilde{Q}_{air}$ is 0.89, significant at the 99% confidence level. In comparison, the mean ocean advective heat flux ($\tilde{Q}_{adv}$) shows less seasonal variation and has a much smaller magnitude compared to the mean $\tilde{Q}_{air}$. The $\tilde{Q}_{adv}$ in 2011–2012 was smaller with anomalies ranging from −0.01 to 0°C/d and cools the temperature, which counteracts the observed

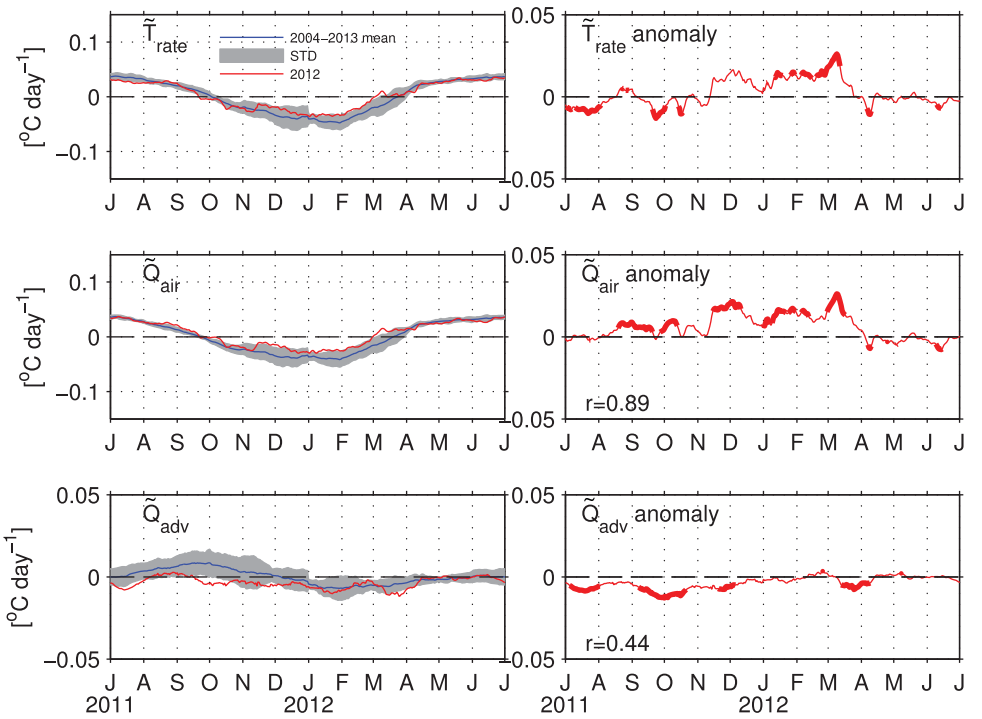

Figure 7. The temperature budget terms comparing 2004–2013 mean and 2011–2012 condition for the GoM. (left) The total rate of changes in 2011–2012 (red) and 2004–2013 (blue) and (right) the anomalous rate of changes in 2011–2012 relative to the 2004–2013 mean. Shaded area in the left figures demonstrates 1 standard deviation (STD) in 2004–2013. Anomalies exceeding 1 STD are highlighted by thick lines in the right figures. Linear correlation coefficients between anomalies of $\tilde{Q}_{air}$ and $\tilde{Q}_{adv}$ and anomaly of $\tilde{T}_{rate}$ are shown in the middle and bottom right figures.

anomalous warming. Note that the $\tilde{Q}_{adv}$ in 2011–2012 does not show clear seasonal variations, which are evident in the 2004–2013 mean.

It is interesting to further distinguish which process, the along-shelf advection or the cross-shelf advection contributed to the negative anomaly of $\tilde{Q}_{adv}$ in 2011–2012. For a control volume, assuming incompressibility, the volume integration of advection terms can be written as follows:

$$\iiint\left(u\frac{\partial T}{\partial x}+v\frac{\partial T}{\partial y}+w\frac{\partial T}{\partial z}\right)dV=\iiint\left(\frac{\partial(uT)}{\partial x}+\frac{\partial(vT)}{\partial y}+\frac{\partial(wT)}{\partial z}\right)dV=\oiint(\mathbf{U}_N T)dS$$
$$=\underbrace{\int_{y_1-h}^{y_2}\int^{\eta}\left(u_2^N T_2-u_1^N T_1\right)dydz}_{(a)}+\underbrace{\int_{x_1-h}^{x_2}\int^{\eta}\left(v_2^N T_2-v_1^N T_1\right)dxdz}_{(b)}+\underbrace{\int_{x_1}^{x_2}\int^{y_2}\left(w_2^N T_2-w_1^N T_1\right)dxdy}_{(c)} \quad (5)$$

The terms (a), (b), and (c) on the right-hand side of the equation are flux divergence terms, where the superscript *N* stands for normal velocity (positive outward) across boundaries. In our s-coordinate model, the vertical advective flux is treated to be perpendicular to the terrain-following layers. Due to no advective flux across the material surfaces at the ocean surface and the seabed, (c) goes to zero. We calculate the horizontal heat flux terms, (a) and (b), at the horizontal boundaries of the GoM/MAB. The lateral boundaries at the shelf edge are chosen to be along the 200 m isobath (black line in Figure 2), and those on the shelf (black dashed lines, Figure 2) are chosen to be perpendicular to the local 200 m isobath. Cross-shelf divergence is calculated as the lateral heat transport across the 200 m isobaths divided by the volume of the corresponding volumes, while the along-shelf divergence is the difference between the lateral heat transport across the northeast and southwest boundaries divided by the corresponding control volumes.

In the GoM, the 10 year mean along-shelf convergence during November–May varies from 0.01 to 0.03°C/d and the standard deviations are large relative to the means (Figure 8). During November 2011 to May 2012, the along-shelf convergence was smaller than the 2004–2013 mean, with magnitudes up to −0.02°C/d. In

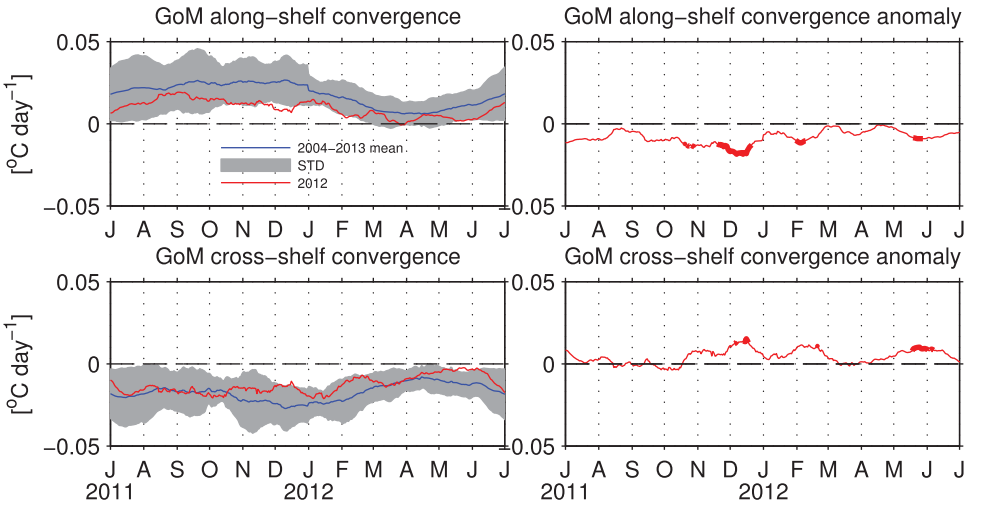

Figure 8. Along-shelf and cross-shelf heat flux convergence for the GoM. (left) The mean values (blue curves) for each term are calculated for the 2004–2013 period. Shaded area denotes 1 standard deviation (STD). (right) Anomalies exceeding 1 STD are highlighted by thick lines.

comparison to the along-shelf heat flux convergence, the cross-shelf convergence during November 2011 to May 2012 was slightly larger than the mean, with anomalies up to 0.02°C/d. Therefore, the negative anomaly of advective flux in the GoM was due to the along-shelf convergence anomaly at the Scotian shelf and northern New England shelf, but neither was significantly different from the 10 year mean except for the periods of November–December 2011 and early February 2012.

In the MAB, the 10 year mean $\tilde{T}_{rate}$ changes from 0 to 0.09°C/d during the warming season April–September to −0.09 to 0°C/d during the cooling season October–March (Figure 9). The $\tilde{T}_{rate}$ during the period of October 2011 to March 2012 was anomalously positive, varying from 0 to 0.04°C/d. This suggests that the MAB water was cooling more slowly than normal during the winter-spring of 2011–2012. $\tilde{Q}_{air}$ during October

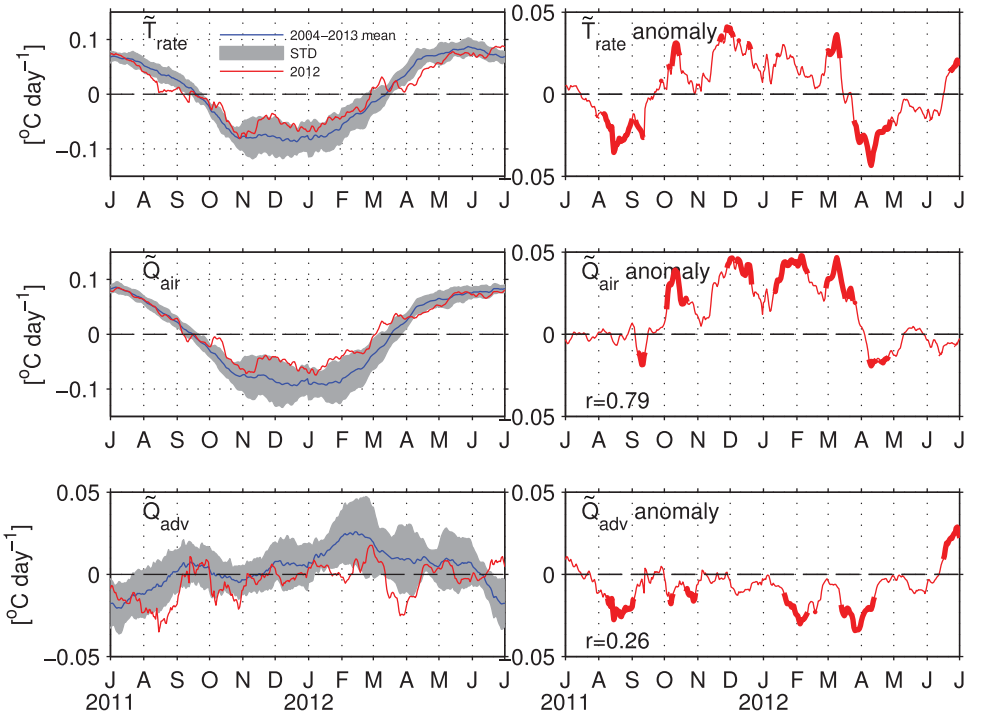

Figure 9. Same as Figure 7, but for the MAB.

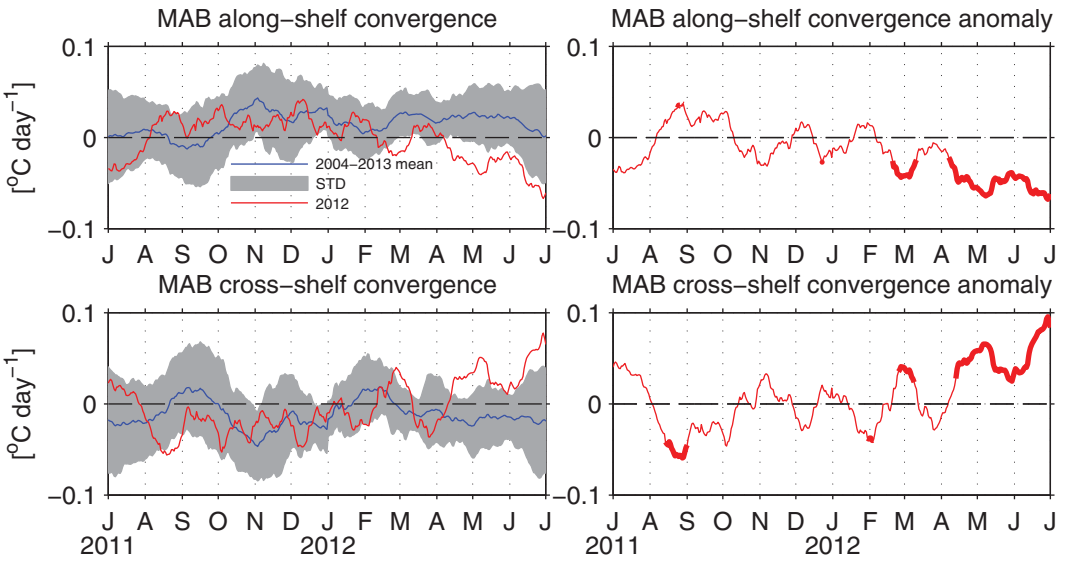

Figure 10. Same as Figure 8, but for the MAB.

2011 to March 2012 was larger than the 10 year mean during the same period, and the magnitude of the anomalies was up to 0.04°C/d. The temporal variations of $\tilde{Q}_{air}$ and $\tilde{T}_{rate}$ roughly resemble each other, with a correlation coefficient of 0.79, and exhibit greater amplitudes than those in the GoM. In comparison, the 10 year mean $\tilde{Q}_{adv}$ in the MAB has less seasonal variation, and the $\tilde{Q}_{adv}$ of 2011–2012 is mostly smaller than the mean. The $\tilde{Q}_{adv}$ during October 2011 to March 2012 was smaller than the mean with anomalies varying between −0.03 and 0°C/d.

We further decompose the total advective flux terms into the along-shelf and cross-shelf convergence terms for the MAB (Figure 10). The 10 year mean along-shelf convergence of heat flux during October–March is 0–0.04°C/d. In the same period of 2011–2012, the along-shelf divergence anomaly varies from −0.04 to 0.03 during October–January, and overall is not significant. The 10 year mean cross-shelf convergence during October–March is −0.05 to 0.01°C/d. During the same period of 2011–2012, the cross-shelf convergence anomaly varies from −0.05 to 0.04°C/d. It seems that both terms contributed to the negative anomalies of the $\tilde{Q}_{adv}$, however, the flux convergence terms are complicated, possibly due to the complexity of the along-shelf and cross-shelf exchange processes in the MAB, which inherently occur over small spatial and temporal scales [*Gawarkiewicz et al.*, 2004]. More importantly, neither anomaly is statistically significant during the period of anomalous $\tilde{T}_{rate}$ except late February and early March.

Collectively, the roles that the air-sea flux and ocean advective flux played during the winter-spring of 2011–2012 in the GoM and the MAB are summarized in Figure 11 as the cumulative volume-averaged temperature budget. Based on (3), for the cumulative volume-averaged temperature anomaly, we have

$$d\tilde{T}^a = \tilde{Q}^a_{airT} + \tilde{Q}^a_{advT} \tag{6}$$

where superscript *a* denotes the anomalies of each term during November 2011 to May 2012. The temperature averaged in the GoM on 1 November 2011 was below the 10 year mean by 0.6°C, however, after the anomalous winter and spring of 2011–2012, the temperature was already 1.3°C above the 10 year mean on 23 March 2012 when the temperature anomaly was at the peak. During this process, the anomalously positive $\tilde{Q}^a_{airT}$ played a critical role to raise the GoM temperature, contributing 2.2°C in contrast to −0.3°C cooling by the ocean advection. For the intraseasonal oscillation of $\tilde{Q}^a_{airT}$ during March–May in 2012 as well as the peak value in March 2012, when the SST over the Northeast coastal ocean was the highest on record (Figure 1), the temperature anomaly closely followed $\tilde{Q}^a_{airT}$. In comparison, $\tilde{Q}^a_{advT}$ was cooling the GoM over this period. Similarly, the temperature in the MAB on 1 November 2011 was just below the 10 year mean by 0.2°C, and by 23 March 2012, the MAB was 2.6°C warmer than the corresponding mean value. Clearly, the warming process was dominated by the anomalous $\tilde{Q}^a_{airT}$ (Figure 11), which contributed as much as 4.8°C

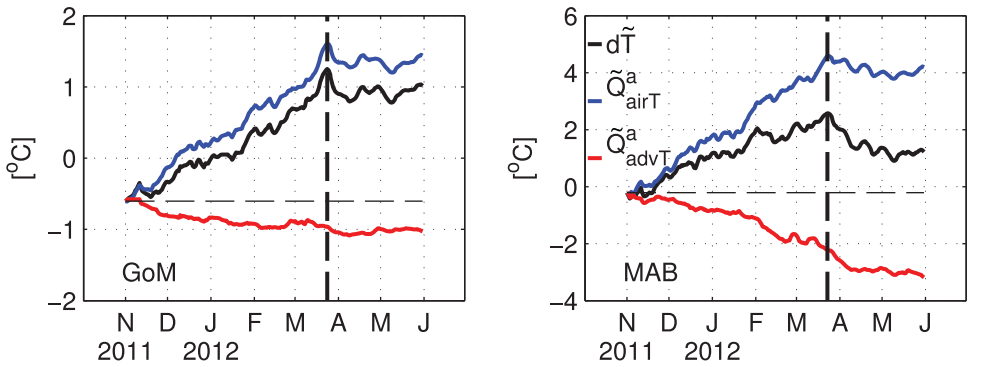

Figure 11. Cumulative volume-averaged temperature anomaly terms (based on equation (6) in the text) for the GoM and MAB during winter-spring of 2011–2012. Vertical dashed line denotes the time when the volume-averaged temperature anomaly is at its maximum.

to the warming. The ocean advection was alleviating the warming caused by the anomalous air-sea flux with a negative contribution of −2°C. Quantitatively, the contribution from the air-sea heat flux contributed 171% (116%) of the anomalous warming for the peak value on 23 March 2012 in the MAB (GoM), whereas the ocean advective heat flux contributed −71% (−16%).

6. Summary

We conducted realistic numerical modeling studies to better understand extreme variability in the coastal ocean during the 2012 warming to explore the underlying dynamics. Overall, the model reproduced the observed thermal structure in the coastal ocean off the Northeast U.S. during the extreme warming period of 2011–2012. Comparisons of surface temperature against NDBC buoys show excellent model skill with linear correlation coefficients higher than 0.97 from the GoM to Virginia Beach. More importantly, the model compares very well against four-dimensional temperature and salinity data from the ECOMON surveys. The observed spatiotemporal characteristics and vertical structure were well reproduced by the model. We diagnosed the dynamical processes underlying this extreme warming event using the model output.

The shelf-wide temperature change during the cooling and warming period of November 2011 to May 2012 was largely controlled by the net air-sea heat flux and was modulated by ocean advective heat flux at more local scales. The evolution of depth-averaged temperature over the seasonal time scale during the extreme event in 2011–2012 was mainly controlled by the air-sea heat flux over the entire Northeast shelf. Ocean advection was cooling most of the subregions during the extreme warm anomaly event, during both the cooling and warming seasons. We note that the Gulf Stream took a northward diversion in October 2011 [*Gawarkiewicz et al*., 2012], but this likely impacted only a limited region near the shelf break south of New England. Further study is necessary to examine both the timing and cross-shelf penetration of the Gulf Stream water mass during the diversion.

Focusing on the anomalies of each term, we diagnosed the volume-averaged temperature for the GoM and MAB, respectively. The slower cooling rate and faster warming rate of ocean temperature during winter and spring of 2011–2012 were dominantly due to the anomalous air-sea heat flux during the same period. Ocean advective heat flux was counteracting the air-sea heat flux, in both the GoM and the MAB. The SST over the western North Atlantic was anomalously large over not just the Northeast U.S. Shelf, but over a large fraction of the source region upstream to the north [see *Mills et al*., 2013, Figure 1], so one might conclude that warmer source waters would drive even more enhanced warming downstream, rather than cooling. However, the warming/cooling of a body of water depends on the heat convergence/divergence rather than just upstream advection. The anomalous cooling due to advective flux in the GoM was primarily caused by the along-shelf divergence of the heat flux, while that in the MAB is modulated by both the along-shelf and cross-shelf heat flux divergence. Further investigation of the along-shelf advective heat flux across the northern boundary (Figure 1) of the GoM reveals that the equatorward heat flux ($\int_{y_1}^{y_2}\int_{-h}^{\eta}(u^N T)dydz$) was smaller during July 2011 to June 2012 compared to the 10 year mean transport during the same period of 2004–2013 (not shown). The equatorward heat flux across the southern boundary of

the GoM (the northern boundary of the MAB) was also smaller compared to the 10 year mean but did not decrease as much as the influx from the northern boundary. This difference explains the along-shelf heat divergence in the GoM (Figure 8). Further calculation of along-shelf transport based on the corrected HYCOM/NCODA data set (see above) reveals that the equatorward transport across the northeast open boundary of the model (from the coast to the 200 m isobaths) was smaller (not shown) during this period, which is consistent with *Hebert et al*. [2013]. This presumably led to the reduced equatorward heat flux downstream at the northern boundary of the GoM. We also note that the equatorward along-shelf heat flux across the southern boundary of the MAB was more variable and did not show any consistent pattern. The complex along-shelf and cross-shelf processes in the MAB [*Chen and He*, 2014, Figure 11] jointly produced the negative anomaly of advective flux in the MAB during this extreme event (Figure 10).

Our study shows that air-sea heat flux anomalies played a critical role during the extreme warm anomaly during 2011–2012. Despite the different approaches, results obtained here using the numerical model are consistent with previous observation-based findings by *Chen et al*. [2014a]. This case study of the unusual extreme event in the coastal ocean offers insights on a linkage between different components in the atmosphere-ocean system and is relevant to the issue of downscaling results from climate scale simulations using Global Circulation Models to continental shelves. For example, the large magnitude of the air-sea fluxes may be consistent with recent suggestions on changes in jet stream dynamics and the meandering due to warming of the Arctic with corresponding effects on the jet stream [*Cohen et al*., 2014; *Francis and Vavrus*, 2012; *Liu et al*., 2012]. It will be intriguing to investigate how the roles of the atmosphere forcing and ocean advection in modulating the temperature might change from year to year.

Acknowledgments

K.C. was supported by the Woods Hole Oceanographic Institution Postdoctoral Scholar program, the Coastal Ocean Institute, and the National Science Foundation (NSF) under grant OCE-1435602. G.G.G. was supported by NSF grants OCE-1435602 and OCE-1129125. Y.-O.K. was supported by the NSF grant OCE-1435602. W.G.Z. was supported by the NSF grant OCE-1129125. We specially thank Dennis McGillicuddy for his contribution to this work, which was supported by the Holger W. Jannasch Chair for Excellence in Oceanography. Comments from Steven Lentz and Kenneth Brink on an early draft were helpful. K.C. thanks Paula Fratantoni for providing the NEFSC polygon data. Constructive comments from two anonymous reviewers are appreciated. Numerical simulations were conducted on the Stampede Supercomputer at the Texas Advanced Computing Center (TACC) with support from the NSF Extreme Science and Engineering Discovery Environment (XSEDE) Startup Allocation (OCE130031). Data used in this work are available upon request at kchen@whoi.edu.

References

Brink, K. H., R. C. Beardsley, R. Limeburner, J. D. Irish, and M. Caruso (2009), Long-term moored array measurements of currents and hydrography over Georges Bank: 1994–1999, *Prog. Oceanogr.*, *82*(3), 191–223, doi:10.1016/j.pocean.2009.07.004.

Chapman, D. C. (1985), Numerical treatment of cross-shelf open boundaries in a barotropic coastal ocean model, *J. Phys. Oceanogr.*, *15*(8), 1060–1075, doi:10.1175/1520-0485(1985)015<1060:NTOCSO>2.0.CO;2.

Chassignet, E. P., H. E. Hurlburt, O. M. Smedstad, G. R. Halliwell, P. J. Hogan, A. J. Wallcraft, R. Baraille, and R. Bleck (2006), The HYCOM (HYbrid Coordinate Ocean Model) data assimilative system, *J. Mar. Syst.*, *65*(1–4), 60–83.

Chen, K., and R. He (2010), Numerical investigation of the Middle Atlantic Bight shelfbreak frontal circulation using a high-resolution ocean hindcast model, *J. Phys. Oceanogr.*, *40*(5), 949–964, doi:10.1175/2009JPO4262.1.

Chen, K., and R. He (2014), Mean circulation in the coastal ocean off northeastern North America from a regional-scale ocean model, *Ocean Sci. Discuss.*, *11*(6), 2755–2790, doi:10.5194/osd-11-2755-2014.

Chen, K., G. G. Gawarkiewicz, S. J. Lentz, and J. M. Bane (2014a), Diagnosing the warming of the Northeastern U.S. Coastal Ocean in 2012: A linkage between the atmospheric jet stream variability and ocean response, *J. Geophys. Res. Oceans*, *118*, 1–10, doi:10.1002/2013JC009393.

Chen, K., R. He, B. S. Powell, G. G. Gawarkiewicz, A. M. Moore, and H. G. Arango (2014b), Data assimilative modeling investigation of Gulf Stream Warm Core Ring interaction with continental shelf and slope circulation, *J. Geophys. Res. Oceans*, *119*, 5968–5991, doi:10.1002/2014JC009898.

Cohen, J., et al. (2014), Recent Arctic amplification and extreme mid-latitude weather, *Nat. Geosci*, *7*(9), 627–637, doi:10.1038/ngeo2234.

Coumou, D., and S. Rahmstorf (2012), A decade of weather extremes, *Nat. Clim. Change*, *2*(7), 491–496.

Fairall, C. W., E. F. Bradley, J. E. Hare, A. A. Grachev, and J. B. Edson (2003), Bulk parameterization of air–sea fluxes: Updates and verification for the COARE algorithm, *J. Clim.*, *16*(4), 571–591, doi:10.1175/1520-0442(2003)016<0571:BPOASF>2.0.CO;2.

Francis, J. A., and S. J. Vavrus (2012), Evidence linking Arctic amplification to extreme weather in mid-latitudes, *Geophys. Res. Lett.*, *39*, L06801, doi:10.1029/2012GL051000.

Friedland, K. (2012), Ecosystem advisory for the northeast shelf large marine ecosystem. *Advis. 2012 No. 2*, Northeast Fishery Science Center, Woods Hole, Mass.

Garvine, R. W., K. C. Wong, and G. G. Gawarkiewicz (1989), Quantitative properties of shelfbreak eddies, *J. Geophys. Res.*, *94*(C10), 14,475–414,483, doi:10.1029/JC094iC10p14475.

Gawarkiewicz, G., K. H. Brink, F. Bahr, R. C. Beardsley, M. Caruso, J. F. Lynch, and C.-S. Chiu (2004), A large-amplitude meander of the shelfbreak front during summer south of New England: Observations from the Shelfbreak PRIMER experiment, *J. Geophys. Res.*, *109*, C03006, doi:10.1029/2002JC001468.

Gawarkiewicz, G., G. Lawson, M. Petruny-Parker, P. Fratantoni, and J. Hare (2013), The shelf break ecosystem off the Northeastern United States: Current issues and recommended research directions, report, 29 pp., Coop. Inst. for the North Atl. Reg., CINAR, Woods Hole, Mass. [Available at http://www.cinar.org/.]

Gawarkiewicz, G. G., R. E. Todd, A. J. Plueddemann, M. Andres, and J. P. Manning (2012), Direct interaction between the Gulf Stream and the shelfbreak south of New England, *Sci. Rep.*, *2*, 553, doi:10.1038/srep00553.

Haidvogel, D. B., et al. (2008), Ocean forecasting in terrain-following coordinates: Formulation and skill assessment of the Regional Ocean Modeling System, *J. Comput. Phys.*, *227*(7), 3595–3624, doi:10.1016/j.jcp.2007.06.016.

Hall, M. M., and H. L. Bryden (1982), Direct estimates and mechanisms of ocean heat transport, *Deep Sea Res., Part A*, *29*(3), 339–359, doi:10.1016/0198-0149(82)90099-1.

Hansen, J., M. Sato, and R. Ruedy (2012), Perception of climate change, *Proc. Natl. Acad. Sci. U. S. A.*, *109*, E2415–E2423, doi:10.1073/pnas.1205276109.

Hebert, D., R. Pettipas, D. Brickman, and M. Dever (2013), Meteorological, sea ice and physical oceanographic conditions on the Scotian Shelf and in the Gulf of Maine during 2012, *Rep. 2013/058*, 89 pp., Can. Sci. Advis. Sec., Ottawa, Canada.

Lentz, S. J. (2010), The mean along-isobath heat and salt balances over the Middle Atlantic Bight continental shelf, *J. Phys. Oceanogr.*, *40*(5), 934–948, doi:10.1175/2009JPO4214.1.

Lentz, S. J., R. C. Beardsley, J. D. Irish, J. Manning, P. C. Smith, and R. A. Weller (2003), Temperature and salt balances on Georges Bank February–August 1995, *J. Geophys. Res.*, *108*(C11), 8006, doi:10.1029/2001JC001220.

Liu, J., J. A. Curry, H. Wang, M. Song, and R. M. Horton (2012), Impact of declining Arctic sea ice on winter snowfall, *Proc. Natl. Acad. Sci. U. S. A.*, *109*, 4074–4079, doi:10.1073/pnas.1114910109.

Luettich, R. A., J. J. Westerink, and N. W. Scheffner (1992), ADCIRC: An advanced three-dimensional circulation model for shelves, coast, and estuaries. Report 1. Theory and methodology of ADCIRC-2DDI and ADCIRC-3DL, *Tech. Rep. DPR-92-6*, 137 pp., U.S. Army Corps of Eng., Washington, D. C.

Mason, E., J. Molemaker, A. F. Shchepetkin, F. Colas, J. C. McWilliams, and P. Sangrà (2010), Procedures for offline grid nesting in regional ocean models, *Ocean Modell.*, *35*(1–2), 1–15, doi:10.1016/j.ocemod.2010.05.007.

Mills, K., et al. (2013), Fisheries management in a changing climate: Lessons from the 2012 ocean heat wave in the Northwest Atlantic, *Oceanography*, *26*, 191–195, doi:10.5670/oceanog.2013.27.

Montgomery, R. B. (1972), Comments on "Seasonal variability of the Florida Current," by Niiler and Richardson, *J. Mar. Res.*, *32*, 533–535.

Orlanski, I. (1976), A simple boundary condition for unbounded hyperbolic flows, *J. Comput. Phys.*, *21*(3), 251–269.

Peterson, T. C., M. P. Hoerling, P. A. Stott, and S. C. Herring (Eds.) (2013), Explaining Extreme Events of 2012 from a Climate Perspective, *Bull. Amer. Meteor. Soc.*, *94*, S1–S74, doi:10.1175/BAMS-D-13-00085.1.

Rahmstorf, S., and D. Coumou (2011), Increase of extreme events in a warming world, *Proc. Natl. Acad. Sci. U. S. A.*, *108*, 17905–17909, doi:10.1073/pnas.1101766108.

Rayner, N. A., D. E. Parker, E. B. Horton, C. K. Folland, L. V. Alexander, D. P. Rowell, E. C. Kent, and A. Kaplan (2003), Global analyses of sea surface temperature, sea ice, and night marine air temperature since the late nineteenth century, *J. Geophys. Res.*, *108*(D14), 4407, doi:10.1029/2002JD002670.

Reynolds, R. W., T. M. Smith, C. Liu, D. B. Chelton, K. S. Casey, and M. G. Schlax (2007), Daily high-resolution-blended analyses for sea surface temperature, *J. Clim.*, *20*(22), 5473–5496, doi:10.1175/2007JCLI1824.1.

Schauer, U., and A. Beszczynska-Möller (2009), Problems with estimation and interpretation of oceanic heat transport—Conceptual remarks for the case of Fram Strait in the Arctic Ocean, *Ocean Sci.*, *5*(4), 487–494, doi:10.5194/os-5-487-2009.

Shchepetkin, A. F., and J. C. McWilliams (2005), The regional oceanic modeling system (ROMS): A split-explicit, free-surface, topography-following-coordinate oceanic model, *Ocean Modell.*, *9*(4), 347–404, doi:10.1016/j.ocemod.2004.08.002.

Shearman, R. K., and S. J. Lentz (2010), Long-term sea surface temperature variability along the U.S. east coast, *J. Phys. Oceanogr.*, *40*, 1004–1016.

Smith, T. M., R. W. Reynolds, T. C. Peterson, and J. Lawrimore (2008), Improvements to NOAA's Historical Merged Land–Ocean Surface Temperature Analysis (1880–2006), *J. Clim.*, *21*(10), 2283–2296, doi:10.1175/2007JCLI2100.1.

Todd, R. E., G. G. Gawarkiewicz, and W. B. Owens (2012), Horizontal scales of variability over the Middle Atlantic Bight shelf break and continental rise from finescale observations, *J. Phys. Oceanogr.*, *43*(1), 222–230, doi:10.1175/JPO-D-12-099.1.

Warner, J. C., C. R. Sherwood, H. G. Arango, and R. P. Signell (2005), Performance of four turbulence closure models implemented using a generic length scale method, *Ocean Modell.*, *8*(1–2), 81–113, doi:10.1016/j.ocemod.2003.12.003.

Wilkin, J. L., and E. J. Hunter (2013), An assessment of the skill of real-time models of Mid-Atlantic Bight continental shelf circulation, *J. Geophys. Res. Oceans*, *118*, 2919–2933, doi:10.1002/jgrc.20223.